Infrared optical constants of orthorhombic IV-VI lamellar semiconductors refined by a combined study using optical and electronic spectroscopies

Li-Ming Yu, A. Degiovanni, P. A. Thiry, J. Ghijsen, and R. Caudano
Laboratoire Interdisciplinaire de Spectroscopie Electronique, Institute for Studies in Interface Sciences, Facultés Universitaires Notre-Dame de la Paix, Rue de Bruxelles 61, B-5000 Namur, Belgium

Ph. Lambin
Laboratoire de Physique des Solides, Institute for Studies in Interface Sciences, Facultés Universitaires Notre-Dame de la Paix, Rue de Bruxelles 61, B-5000 Namur, Belgium
(Received 9 November 1992)

Cleaved surfaces of the IV-VI lamellar semiconducting compounds GeS, GeSe, SnS, and SnSe have been studied by high-resolution electron-energy-loss spectroscopy (HREELS). The infrared optical constants of the materials were obtained by using the dielectric theory taking into account the resonance frequencies published from infrared reflectivity (IRS) data. The limitations of the HREELS and IRS measurements in the case of these materials are discussed in detail. It is shown that, by combining the information from both spectroscopies, it is possible to determine better some of the oscillator strengths of these materials. In addition to a linear relationship between the phonon frequencies of GeSe and GeS, and SnSe and SnS, a similar relationship was also found between their oscillator strengths, which may provide an improved understanding of the lattice properties of these lamellar compounds.

I. INTRODUCTION

Among the IV-VI semiconductor compounds, germanium sulfide (GeS), germanium selenide (GeSe), tin sulfide (SnS), and tin selenide (SnSe) have the layered orthorhombic structure with eight atoms per unit cell forming biplanar layers normal to the largest c axis.[1] The atoms in a single layer are joined to three nearest neighbors by covalent bonds which form zigzag chains along the b axis while there is only van der Waals bonding between the layers. This typical crystalline structure results in strong anisotropic optical properties at low energies and more isotropic optical properties at higher energies, which makes them interesting materials intermediate between two-dimensional and three-dimensional semiconductors.

A variety of methods including photoemission, electron-energy-loss spectroscopy, and ellipsometry have been applied to study these anisotropic properties.[2–4] As far as lattice vibrations are concerned, a group factor analysis of the three-dimensional space group D_{2h}^{16} of IV-VI lamellar compounds predicts the existence of 21 optical phonons, among which 2 are optically inactive, 7 are infrared active, and 12 are Raman active. Because of the existence of an inversion center lying between the double layers, one should expect the Raman and infrared-active phonons to be nondegenerate. On the other hand, in the limiting case of a layered structure, the two-dimensional symmetry of these materials belongs to DG32 in Woods notation[19] with no inversion center; therefore a near degeneracy of some infrared- and Raman-active phonons is expected because the coupling between layers can be ignored.

Raman scattering and infrared transmission and reflection experiments were employed in the 1970s[5–9] to study the splitting of the corresponding infrared- and Raman-active modes. Because optical spectroscopies provide a good spectral resolution, the phonon energies obtained by these experiments were quite in agreement and thus the ratios of interlayer and intralayer interactions were well estimated in the published papers. On the other hand, the other optical parameters, such as oscillator strength, were poorly determined by Kramers-Kronig (KK) analysis of infrared reflectivity data, especially in the case of the electric field of the optical beam being parallel to the c axis, which will be discussed in detail in the next section. In other words, we consider that the TO phonon frequencies of these IV-VI materials have been better determined by infrared reflectivity spectroscopy (IRS), compared to the other parameters, such as oscillator strength, in their dielectric functions. The subject of this paper is to refine the oscillator strength values of these materials with the help of high-resolution electron-energy-loss spectroscopy (HREELS) measurements.

II. DIELECTRIC CONSTANTS FROM INFRARED REFLECTIVITY DATA

In order to have a clear mind about what can be obtained from a KK analysis or an oscillator fit of infrared reflectivity data, it is worthwhile to overview their corresponding data treatments. The published infrared reflectivity spectra of GeS, GeSe, SnS, and SnSe are plotted in Fig. 1 with open dots. By assuming constant reflectivity below 20 cm^{-1} and above 4000 cm^{-1}, a KK integration was performed, giving the phase angle of the complex reflectivity. The real and imaginary parts ε_{j1} and ε_{j2} of the complex dielectric function $\varepsilon_j(\omega)$ along the principal optical axis j were then calculated by inverting Fresnel's formula for reflection.[10] The resulting plots can

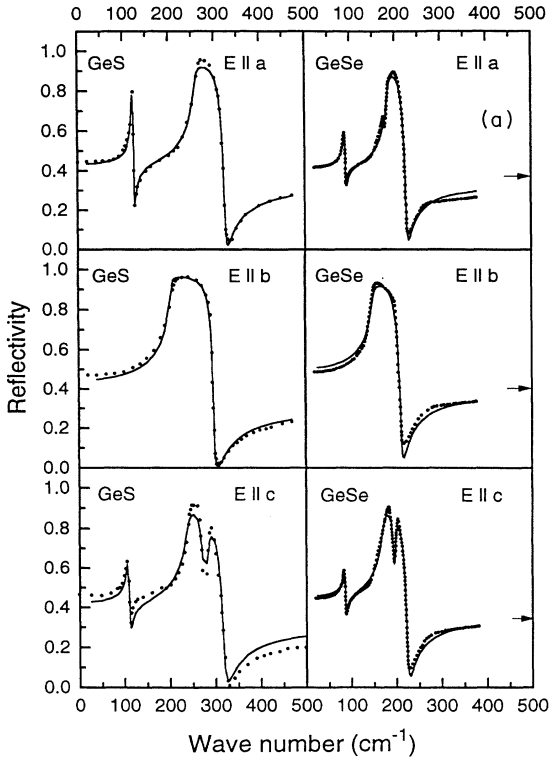

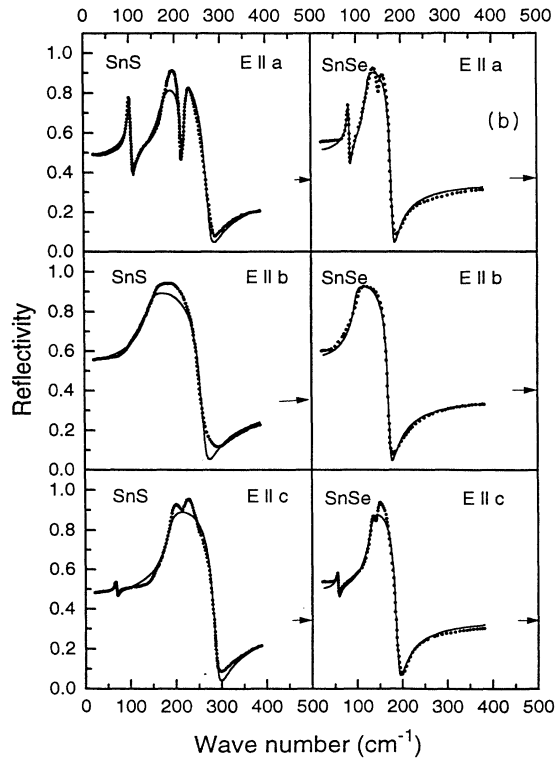

FIG. 1. (a) Infrared reflectivity data of GeS and GeSe with their oscillator fit. (b) Infrared reflectivity data of SnS and SnSe with their oscillator fit.

be found in Refs. 5–8. The dangers and difficulties of associating particular features in ε_1 and ε_2 with phonon energies where the phonons are closely spaced and/or heavily damped have been emphasized by Barker.[11] For their special purposes, the authors of Refs. 5–8 all adopted Barkers' approximation and assumed the maxima in the ε_2 spectra occurring at the TO phonon frequencies and the above-resonance zero crossings of ε_1 occurring at LO phonon frequencies. Unfortunately, for all of these four materials, there are resonances for which ε_1 exhibits no zero crossing, which means that no truly longitudinal vibration exists in these cases. Nevertheless, some authors[5] still estimated LO phonon frequencies by considering where the zero crossing would have occurred if the damping were lower. Other authors[7,8] determined LO frequencies from the poles of the dielectric function $\mathrm{Im}(-1/\varepsilon)$.

Due to the fact that the complex dielectric function along the j axis of the materials can be expressed either with TO and LO phonon frequencies or with an oscillator model by using the sum rule,

$$\varepsilon_j = \varepsilon_{j1} + i\varepsilon_{j2} \tag{1}$$

$$= \varepsilon_\infty \prod_k \frac{\omega_{\mathrm{LO},k}^2 - \omega^2 - i\omega_{\mathrm{LO},k}\omega\gamma_{\mathrm{LO},k}}{\omega_{\mathrm{TO},k}^2 - \omega^2 - i\omega_{\mathrm{TO},k}\omega\gamma_{\mathrm{TO},k}} \tag{2}$$

$$= \varepsilon_\infty + \sum_k \frac{\omega_{\mathrm{TO},k}^2 S_k}{\omega_{\mathrm{TO},k}^2 - \omega^2 - i\omega\omega_{\mathrm{TO},k}\gamma_k}\,, \tag{3}$$

where S_k (≥ 0) is the strength of the kth oscillator along the j axis, while $\omega_{\mathrm{TO},k}$ and $\omega_{\mathrm{LO},k}$ are resonance TO and LO frequencies, respectively. $\gamma_{\mathrm{TO},k}$ and $\gamma_{\mathrm{LO},k}$ are corresponding dimensionless damping ratios, which can be written as γ_k. It is clear that the oscillator strengths could not be well determined if approximate LO phonon frequencies were used. To what extent were these oscillator strengths misattributed? With this question in mind, we tried the oscillator fits with a least-squares optimization program for all of the reflectivity spectra in Fig. 1. The best fitted results appear as solid lines in the figure. The resulting optical constants from KK analysis and oscillator fits are summarized in Table I.

As was pointed out in Refs. 5–8, we found the oscillators fits of reflectivity data failed with the oscillator number prediction from group theory for all of these materials. For GeS and GeSe, only two-oscillator fits were successful for the case of $E\|a$, although we can clearly see a contribution from the missing oscillator on the spectrum of GeSe ($E\|a$). The same situation happened for the spectra of SnS ($E\|c$), SnSe ($E\|c$), and SnSe ($E\|a$). In all of these cases, when we used three oscillators for the curve fitting, negative oscillator strength and/or negative damping factors appeared in the results, so that the fitted reflectivity spectra in Fig. 1 were obtained with only two oscillators for the above-mentioned cases. We believe that this failure comes from possible experimental errors, which may be due to the configuration of the experiments and/or the quality of the material surfaces, especially for the cases of $E\|c$ where one has to cut and polish a surface containing van der Waals bonding. If one of three pre-

TABLE I. Phonon frequencies ω_{TO} and ω_{LO} (in cm^{-1}) and dielectric constants ε_0 and ε_∞ of GeS, GeSe, SnS, and SnSe as determined from a Kramers-Kronig analysis of the reflectivity data between 20 and 4000 cm^{-1}, while ω_j, S_j, γ_j, and ε_∞ are the corresponding infrared optical parameters from the oscillator fits of the same data.

		GeS			GeSe			SnS			SnSe		
		$E\|\|a$	$E\|\|b$	$E\|\|c$	$E\|\|a$	$E\|\|b$	$E\|\|c$	$E\|\|a$	$E\|\|b$	$E\|\|c$	$E\|\|a$	$E\|\|b$	$E\|\|c$
KK	TO_1	117.5	201.0	105.0	88	150	83	99		69	80		56
	LO_1	123.5	298.0	107.0	91.5	210.5	86	107		71	85		57
osc.	ω_1	119.2	202	105	87.8	148.7	83.4	99.5		69.0	82.5		56.0
	S_1	2.5	13.5	2.4	1.7	17.9	1.8	5.7		0.7	4.6		1.9
	γ_1	0.023	0.022	0.05	0.050	0.054	0.053	0.061		0.06	0.044		−0.07
KK	TO_2			237.0	175		172	178		188	123		130
	LO_2			275.0	178		194	215		193	149		141
osc.	ω_2			237			169.7	174		187.3	124.4		130.1
	S_2			7.8			9.8	14.2		17.5	16.0		17.1
	γ_2			0.045			0.054	0.125		0.083	0.065		0.086
KK	TO_3	257.5		280	186		198	222	145	220	150	96	142
	LO_3	325.0		320.0	224		221	277	265	289	180	172	191
osc.	ω_3	257.7		279.7	184.5		169.9	221.7	142			97.1	
	S_3	7.6		0.55	6.62		0.43	0.76	33.6			35.9	
	γ_3	0.027		0.04	0.040		0.030	0.029	0.137			0.091	
KK	ε_0	25.1	29.5	30.0	21.9	30.4	25	32	48	32	45	62	42
	ε_∞	14.8	12.0	10.0	18.7	21.9	14	14	16	16	13	17	16
osc.	ε_∞	13.6	11.8	12.0	13.7	17.5	15.0	11.7	13.9	12.8	15.7	16.6	15.4

dicted oscillators had a very low strength, a strong damping, or a near degeneracy with one of the other two phonons, the possible experimental errors in these spectra could cause the fitting failure. It must be emphasized that no such problems are encountered in a KK analysis, because, in this latter case, no model is requested and no fitting is performed. Moreover, KK integration can bring a local experimental error to the whole spectral range.

Nevertheless, plotting the corresponding infrared-active frequencies of GeSe vs GeS as well as that of SnSe vs SnS, Chandrasekar *et al.* found a linear correlation (Fig. 2). According to the arguments in Ref. 8, the ratio of the corresponding frequencies (labeled ν_j) of two lamellar compounds α and β of the IV-VI family follows the relation

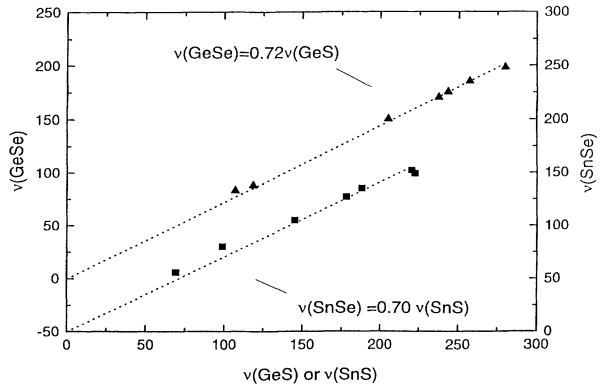

FIG. 2. Linear correlation of optical TO frequencies between GeS and GeSe and between SnS and SnSe.

$$\frac{\nu_{j\alpha}}{\nu_{j\beta}} = \frac{r_\alpha^{-2.2} M_\alpha^{-0.5}}{r_\beta^{-2.2} M_\beta^{-0.5}}, \tag{4}$$

where $r_{\alpha,\beta}$ and $M_{\alpha,\beta}$ are the lattice constant and atomic mass, respectively. There is no such relation for ν(GeS) vs ν(SnS) or ν(GeSe) vs ν(SnSe). In fact, all the infrared- and Raman-active vibration frequencies follow the same linear relation, so that we can be sure of the TO frequencies values from the optical measurements. According to this linear relation, the missing line of GeS in the spectrum of $E\|a$ could be assigned at 243 cm^{-1} by inserting the corresponding TO frequency of GeSe at 175 cm^{-1} into the relation in Fig. 2, though it was reported at 315 cm^{-1} by an infrared reflectivity experiment at 77 K.[9] There is no reason why this low-intensity mode should be an exception.

III. CHARACTERISTICS OF THE HREELS SPECTRUM OF AN ANISOTROPIC UNIAXIAL MATERIAL

HREELS has been widely used to probe various kinds of vibrational modes of surface elementary excitations such as plasma oscillations, long-wavelength optical phonons (Fuchs-Kliewer modes), and adsorbate vibrations.[12] Among the two possible electron-surface interaction mechanisms involved in an inelastic-scattering event, dipole scattering prevails for low-energy electrons reflected near the specular direction.[13] Due to a long-range Coulomb interaction between the moving electron and the polarization potential of the target inside a thickness of about 100 Å, the HREELS spectrum gives a set of loss and gain peaks related to the surface excitations. An analytical description of the corresponding elementary

TABLE II. Oscillator parameters ω_j (in cm^{-1}), S_j, and γ_j and dielectric constants ϵ_∞ of GeS, GeSe, SnS, and SnSe as determined from HREELS data.

	GeS			GeSe			SnS			SnSe		
	$E\|\|a$	$E\|\|b$	$E\|\|c$	$E\|\|a$	$E\|\|b$	$E\|\|c$	$E\|\|a$	$E\|\|b$	$E\|\|c$	$E\|\|a$	$E\|\|b$	$E\|\|c$
ω_1	120	202	106	88	149	83	99		69	80		56
S_1	2.6	14.0	2.2	2.2	12.5	2.0	5.7		1.0	4.6		1.2
γ_1	0.035	0.04	0.03	0.06	0.08	0.035	0.06		0.06	0.06		0.06
ω_2	243		237	175		172	174		187.3	123		130
S_2	0.4		7.8	0.4		7.2	14.2		14.5	13.2		13.5
γ_2	0.03		0.05	0.045		0.12	0.13		0.12	0.09		0.08
ω_3	258		280	186		198	221.7	142	220	149	97	152
S_3	7.6		0.6	7.0		0.5	0.76	34.5	3.9	0.7	32.5	2.8
γ_3	0.045		0.025	0.10		0.025	0.05	0.14	0.025	0.06	0.09	0.05
ε_0	24.2	25.8	20.6	23.3	28.0	23.7	32.4	48.4	32.3	34.2	49.1	32.9
ε_∞	13.6	11.8	10.0	13.7	15.5	14.0	11.7	13.9	12.8	15.7	16.6	15.4

surface excitation probability can be predicted by the classical loss function $P_{cl}(\omega)$ in the framework of the dielectric theory,[14]

$$P_{cl}(\omega)=\frac{4}{\pi^2}\frac{e^2}{\hbar v_\perp}\int_D \frac{(kv_\perp)^3}{[(\omega-\mathbf{k}\cdot\boldsymbol{v}_\parallel)^2+(kv_\perp)^2]^2} \times \mathrm{Im}\left[\frac{-1}{1+\xi(\mathbf{k},\omega)}\right]\frac{d^2k}{k^2}, \quad (5)$$

where $\boldsymbol{v}_\parallel$ and $v_\perp$ are the electron velocity components parallel and perpendicular to the target surface, respectively. ξ is the so-called effective surface dielectric function valid for a semi-infinite anisotropic crystal,[15]

$$\xi(\mathbf{k},\omega)=[\varepsilon_{zz}\mathbf{k}^0\cdot\varepsilon_{\rho\rho}\mathbf{k}^0-(\varepsilon_{\rho z}\mathbf{k}^0)^2]^{1/2}, \quad (6)$$

where $\mathbf{k}^0=\mathbf{k}/|k|$ and $\varepsilon_{\rho\rho}$, $\varepsilon_{\rho z}$, and ε_{zz} are extracted from the dielectric tensor of the target material, the z axis being oriented normal to the surface whereas $\rho=(x,y)$ is a two-dimensional vector parallel to the surface. The dielectric tensor of the semi-infinite anisotropic substrate is fully characterized by its three principal components $\varepsilon_j(\omega)$ in formula (1)–(3). Taking account of finite temperature effects, a "bosonization" process is applied and the complete experimental spectrum can finally be simulated.[16]

For a crystal of the orthorhombic symmetry with a free surface perpendicular to the c axis, Eq. (6) reduces to $\xi(\mathbf{k},\omega)=[\varepsilon_c(\varepsilon_a k_x^2+\varepsilon_b k_y^2)/k^2]^{1/2}$, the k_x and k_y components of the surface wave vector being along the a and b axes, respectively. This expression mixes contributions of the dielectric tensor from the principal axis along c with those parallel to the surface. HREELS therefore gives access to optical parameters for directions both parallel and perpendicular to the surface of a cleaved sample, which is well characterized and does not require a complicated surface preparation. By contrast, IRS has to use noncleavable surfaces in order to obtain information along the c axis.

In the present HREELS experiments, we used a detector with a circular aperture. The domain of surface wave vectors that inelastically scatter the electrons into the acceptance angle of the detector is an ellipse having its major axis oriented perpendicular to the incidence plane. As a consequence of the dielectric anisotropy of the crystal, one would therefore expect observing variations in the loss spectra when the incidence plane is rotated around the normal direction. For the IV-VI lamellar materials under investigation here, there are in fact little anisotropic effects. This is demonstrated both experimentally and theoretically in Fig. 3, where we compare HREELS spectra from the GeS(001) surface taken with the incident

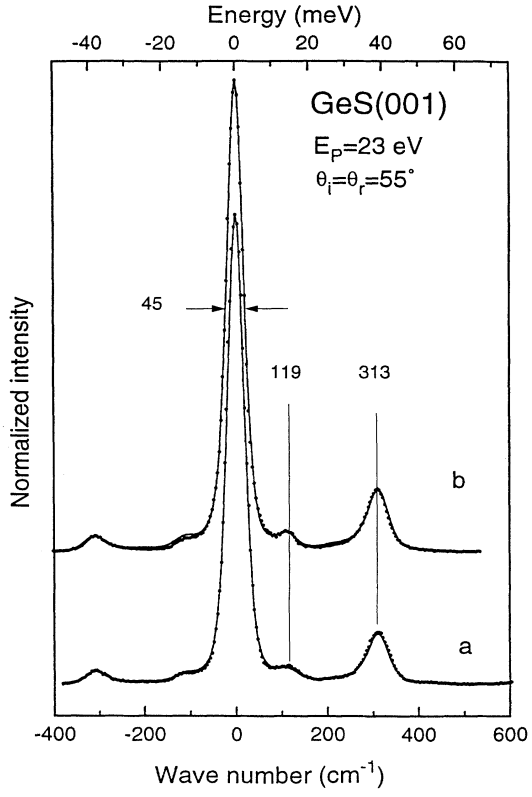

FIG. 3. HREELS spectra of GES with incident beam in (a) a-c plane and in (b) b-c plane, where dots represent the experimental data and solid lines are simulated spectra.

electron beam coming in the a-c or b-c planes. The experimental spectra are shown as dotted lines in Fig. 3 with their theoretical simulation curves represented by solid lines. The strong peak at 313 cm^{-1} is a surface Fuchs-Kliewer phonon. Such a mode can propagate along the a (b) axis only when ε_c and ε_a (ε_b) are both negative. The frequency of the mode must then satisfy the equation $\varepsilon_a(\omega)\varepsilon_c(\omega)=1$ ($\varepsilon_b\varepsilon_c=1$). With the data of Table II and neglecting here any damping, one finds $\omega=323$ or 298 cm^{-1} for $\mathbf{k}\|a$ or b, respectively. With the energy resolution realized here, this anisotropic surface phonon leads to a single loss peak at the average position of 313 cm^{-1} that is found independent on the azimuthal angle of the electron beam, even though the elliptical domain of wave vectors favors k_x components over k_y, or vice versa, when the incidence plane is rotated from the a to the b direction.

The loss structure observed around 119 cm^{-1} in Fig. 3 originates from continua of bulk modes that exist when ε_c and ε_a ($\mathbf{k}\|a$) or ε_c and ε_b ($\mathbf{k}\|a$) have opposite signs. A continuum of this sort exists when $106<\omega<111$ cm^{-1} (first reststrahlen of ε_c according to Table II) for all the directions of $\mathbf{k}$. Another continuum takes place in the interval (120,126) cm^{-1} for $\mathbf{k}\|a$ (first reststrahlen of ε_a) but does not exist for $\mathbf{k}\|b$. The close proximity of these two continua causes the anisotropy of the target spectral function to have little influence on the HREELS spectrum.

IV. EXPERIMENTAL DETAILS

The experiments reported here were performed in a two-chamber system consisting of a preparation and an analyzer chamber with base pressure of 10^{-10} Torr. The HREELS spectrometer (SEDRA-ISA Riber) combines two 180°-hemispherical electrostatic capacitors used as monochromator and analyzer, respectively. The analyzer can be turned over 100°, which enables us to change the incidence angle from 40° to 85°. The GeS, GeSe, $SnS_{0.9}Se_{0.1}$, and SnSe samples were undoped single crystals grown by the vacuum sublimation method.[17] These crystals are easily cleaved along the a-b plane since the van der Waals bonding is directed along the c axis. For the same reason, the surfaces were quite stable and no contamination could be observed on the *in situ* cleaved surface even after several days. The orientation and lattice constants of cleaved crystals were checked by low-energy electron diffraction (LEED), and the sample was mounted on a rotatable sample holder which enabled us to align the a or b axis in the incidence plane of the HREELS spectrometer.

V. HREELS RESULTS AND DISCUSSION

In order to demonstrate the accuracy of the optical parameters obtained from a HREELS spectrum, the experiments were done systematically on GeS single crystals with different azimuths and incidence angles and different electron-beam energies. The experimental curves for a primary energy of 23 eV and an incidence angle of 55° are shown in Fig. 3 and the best experimental results (i.e., higher resolution and counting rate) at the optimum conditions are shown in Fig. 4(a) as a dotted line. A simulated curve (dashed line) is also shown in the same figure by inserting the optical constants obtained by oscillator fitting of the reflectivity spectra. A small deviation is observed and the Fuchs-Kliewer (surface and bulk modes) frequencies are observed near 119 and 313 cm^{-1}. The spectrometer function used in the simulation was predetermined by fitting the elastic peak to a mixture of asymmetric Gaussian and Lorentzian. The simulated spectrum was obtained by convoluting this instrumental function with the bosonized loss probability.

As soon as one starts to determine optical parameters from a HREELS spectrum by the above described simulation, the limitation of this method appears clearly. Only two Fuchs-Kliewer loss peaks can be identified on the spectrum, but there are so many parameters to be adjusted that the results cannot be unique. Thanks to the infrared reflectivity measurements, we can fix all the resonance frequencies, the parameters left to be adjusted being the oscillator strengths and damping ratios. By increasing the oscillator strength S_j, the corresponding loss intensity increases as well as its Fuchs-Kliewer frequency. On the other hand, the damping ratio can only affect the width of the peaks when it is kept under a reasonable level, say γ smaller than 0.15. ε_∞ is another insensitive pa-

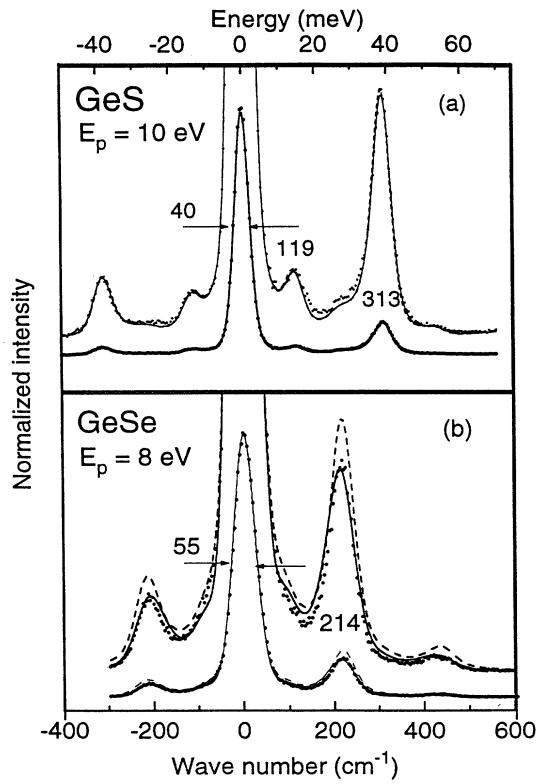

FIG. 4. HREELS spectra of (a) GeS and (b) GeSe under optimum conditions, where dots represent the experimental data, dashed lines are simulated spectra with the optical parameters from infrared reflectivity measurements, and solid lines are simulated spectra.

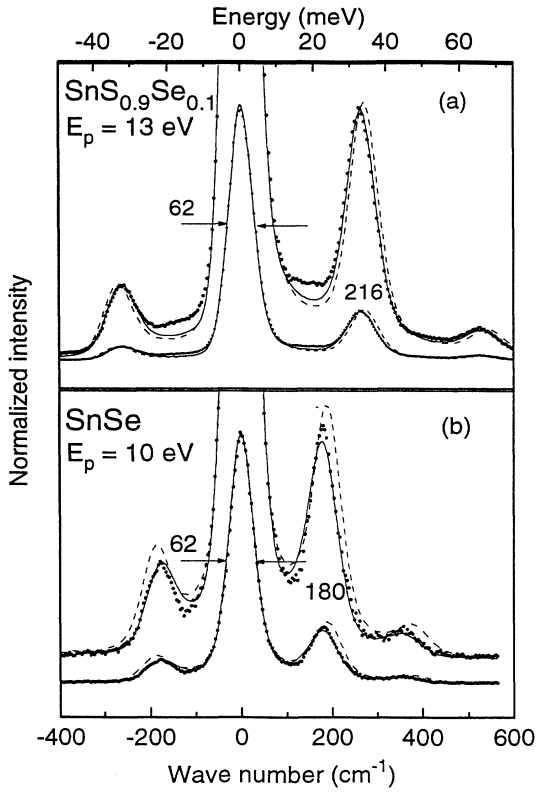

FIG. 5. HREELS spectra of (a) SnS and (b) SnSe. Dots represent the experimental data and dashed lines are simulated spectra with the optical parameters from infrared reflectivity measurements; solid lines are simulated spectra.

rameter, which we took directly from oscillator fit without adjusting.

Knowing all of these, the optical parameters were adjusted manually close to the infrared data to reach a least-squares optimization. The missing vibration mode at 243 cm^{-1} was also included in the simulation although it did not affect much the resulting spectrum due to its lower oscillator strength. Finally, the HREELS spectrum can be well fitted [Fig. 4(a), solid line]. It is worth pointing out that the theoretical curves plotted in Fig. 3 were simulated with exactly the same parameters but different geometry configuration, which proves that there is no artifact coming from our experimental conditions.

The same procedure was applied to fit the best HREELS spectra of GeSe, $SnS_{0.9}Se_{0.1}$, and SnSe and the results are shown in Figs. 4(b), 5(a), and 5(b), respectively. In contrast to GeS, the simulations with optimized parameters from infrared reflectivity (Table I) all show larger deviations, which can be improved with our above-mentioned procedure. However, for the case of $SnS_{0.9}Se_{0.1}$, we can still find a contribution near 180 cm^{-1} that could not be represented. This is because 10% of the sulfur atoms are substituted by selenium and that peak is caused by tin-selenium bonding, which is not included in our simulation as we used only 7 oscillators of SnS instead of 14 in the fitting process. All the resulting parameters are listed in Table II. By comparing with the set of values of Table I, one finds immediately that the optical parameters of GeS obtained by both optical and HREELS measurements are consistent, which indicates the capabilities of both spectroscopies for optical studies. On the other hand, as we have emphasized before, the optical constants, especially the oscillator strengths and damping factors for GeS, SnS, and SnSe, listed in Table I, were previously obtained with ill-fitting conditions (see Fig. 1). They have been refined by this study, some of them by more than 10%. For example, in the case of GeSe, the oscillator strength for the $E\|b$ mode was refined from 17.9 to 12.5.

Figure 6 plots the oscillator strength of the infrared-active modes of GeS against GeSe and SnS against SnSe, where we can find a near-linear relation. According to Szigeti,[18] the effective dynamical charge $e^*_{j\alpha}$ carried by the vibrating ions in cubic crystals is given for the jth mode of material α by

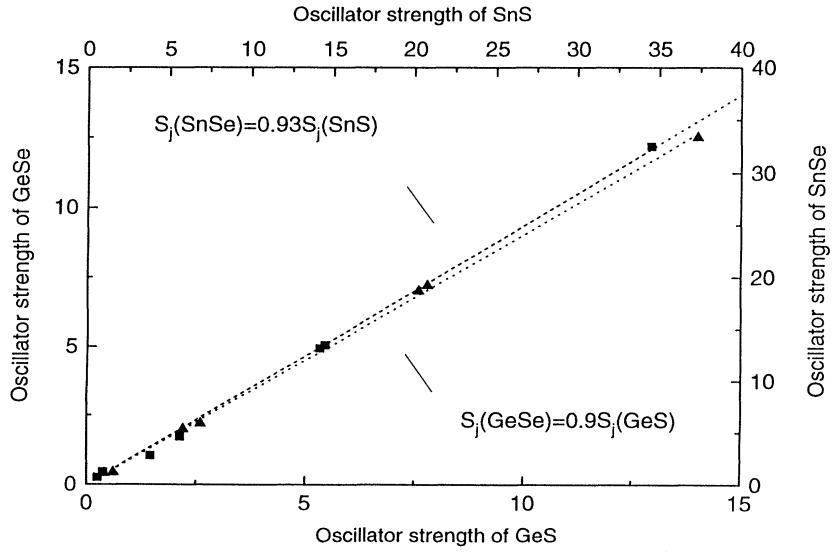

FIG. 6. Linear correlation of the oscillator strengths between GeS and GeSe and between SnS and SnSe.

$$e_{j\alpha}^{*2}=\left[\frac{d\mu_{j\alpha}}{dQ}\right]^2=\frac{9\pi M_\alpha}{N_\alpha(\varepsilon_{\infty\alpha}+2)^2}\nu_{j\alpha}^2 S_{j\alpha}\ , \tag{7}$$

where N_α is the number of oscillators of reduced mass M_α per unit volume. $d\mu_{j\alpha}/dQ$ is the dipole derivative with respect to the vibrational coordinate Q. Taking account of formula (4), one obtains, for the ratio of the corresponding jth oscillator strength of the IV-VI compounds α and β:

$$\frac{S_{j\alpha}}{S_{j\beta}}=\frac{N_\alpha}{N_\beta}\left[\frac{e_{j\alpha}^*}{e_{j\beta}^*}\right]^2\left[\frac{\varepsilon_{\infty\alpha}+2}{\varepsilon_{\infty\beta}+2}\right]^2\left[\frac{r_\alpha}{r_\beta}\right]^{4.4}\ , \tag{8}$$

so that S_j(GeSe) vs S_j(GeSe) and S_j(SnS) vs S_j(SnSe) should be linear, which might mean that formula (7) should still be valid for orthorhombic systems.

VI. CONCLUSIONS

We emphasize that the infrared optical parameters of Table II, resulting from fitting the HREELS spectra with the help of IRS data, represent better values than the ones determined from IRS measurements alone (Table I), especially because all HREELS data were obtained on well characterized cleaved surfaces. "Ideal" reflectivity curves could be produced from the set of refined parameters of Table II. However, one cannot expect these curves to provide a better fit to the IRS data of Fig. 1 because of its above-mentioned experimental limitations. It is interesting to note that the refinement could be obtained only by a close collaboration between HREELS and IRS. On one hand, IRS has a better resolution than HREELS and is needed to provide starting values for the data treatment, but on the other hand HREELS can provide all the dielectric information from well-characterized surfaces, easy to prepare, and stable in ultrahigh-vacuum conditions.

ACKNOWLEDGMENTS

We are grateful to R. L. Johnson for providing us with the samples. We would also like to thank G. Leclerc for his help in the infrared data fitting. J. Ghijsen and Ph. Lambin are supported by the NFSR (Belgium). This work was funded by the Belgian National Program of Interuniversity Research Project on Materials Science initiated by the Belgian State Prime Minister Office (Science Policy Programming).

[1]A. Okazaki, J. Phys. Soc. Jpn. **13**, 1151 (1958); W. Hofmann, Z. Kristallogr. **91**, 161 (1935); A. Okazaki and I. Uada, J. Phys. Soc. Jpn. **11**, 470 (1956).

[2]M. Taniguchi, R. L. Johnson, J. Ghijsen, and M. Cardona, Phys. Rev. B **42**, 3634 (1990).

[3]R. Eymard and A. Otto, Phys. Rev. B **16**, 1616 (1977).

[4]S. Logothetidis, L. Vina, and M. Cardona, Phys. Rev. B **31**, 2180 (1984), S. Logothetidis and H. M. Polatoglou, *ibid.* **36**, 7491 (1986).

[5]J. D. Wiley, W. J. Buckel, and R. L. Schmidt, Phys. Rev. B **13**, 2489 (1976).

[6]P. Mihajlovic, P. M. Nikolic, and H. Hughes, J. Phys. C **9**, L599 (1976).

[7]H. R. Chandrasekar and U. Zwick, Solid State Commun. **18**, 1509 (1976).

[8]H. R. Chandrasekar, R. G. Humphreys, U. Zwick, and M. Cardona, Phys. Rev. B **15**, 2177 (1977).

[9]Yu. A. Mityagin, I. V. Kucherenko, L. K. Vodop'yanov, and V. I. Shtanov, Fiz. Tverd. Tela (Leningrad) **20**, 2974 (1978) [Sov. Phys. Solid State **20**, 1717 (1978)].

[10]W. G. Spitzer and D. A. Kleinman, Phys. Rev. **121**, 1324 (1961).

[11]A. S. Barker, Jr., Phys. Rev. **136**, A1290 (1964).

[12]*Electron Energy Loss Spectroscopy and Surface Vibrations,* edited by H. Ibach and D. L. Mills (Academic, New York, 1982).

[13]P. A. Thiry, M. Liehr, J. J. Pireaux, and R. Caudano, Phys. Scr. **35**, 368 (1987).

[14]Ph. Lambin, J. P. Vigneron, and A. A. Lucas, Phys. Rev. B **32**, 8203 (1985).

[15]A. A. Lucas and J. P. Vigneron, Solid State Commun. **49**, 327 (1984).

[16]Ph. Lambin, J. P. Vigneron, and A. A. Lucas, Comput. Phys. Commun. **60**, 351 (1990).

[17]E. Schönherr, J. Cryst. Growth **57**, 493 (1982).

[18]B. Szigeti, Trans. Faraday Soc. **45**, 155 (1949).

[19]E. A. Wood, Bell Syst. Technol. J. **43**, 541 (1964).